1-1-2018

Several Levels of Theory for Description of Isotope Effects in Ozone: Symmetry Effect and Mass Effect

Alexander Teplukhin
Marquette University

Dmitri Babikov
Marquette University, dmitri.babikov@marquette.edu

Accepted version. *Journal of Physical Chemistry: A*, Vol 122, No. 47 (2018): 9177-9190. DOI.

Several Levels of Theory for Description of Isotope Effects in Ozone: Symmetry Effect and Mass Effect

Alexander Teplukhin
Department of Chemistry, Marquette University, Milwaukee, Wisconsin, United States
Dmitri Babikov
Department of Chemistry, Marquette University, Milwaukee, Wisconsin, United States

Abstract

The essential components of theory for the description of isotope effects in recombination reaction that forms ozone are presented, including the introduction of three reaction pathways for symmetric and asymmetric isotopomers, a brief review of relevant experimental data for singly- and doubly substituted isotopologues, the definitions of ζ-effect and *η*-effect, and the introduction of isotopic enrichment δ. Two levels of theory are developed to elucidate the role of molecular symmetry, atomic masses, vibrational zero-point energies, and rotational excitations in the recombination process. The issue of symmetry is not trivial, since the important factors, such as 1/2 and 2, appear in seven different places in the formalism. It is demonstrated that if all these effects are taken into account properly, then no anomalous isotope effects emerge. At the next level of theory, a model is considered in which one scattering resonance (sitting right at the top of centrifugal barrier) is introduced per ro-vibrational channel. It is found that this approach is equivalent to statistical treatment with

partition functions at the transition state. Accurate calculations using hyper-spherical coordinates show that no isotope effects come from difference in the number of states. In contrast, differences in vibrational and rotational energies lead to significant isotope effects. However, those effects appear to be local, found for the rather extreme values of rotational quantum numbers. They largely cancel when rate coefficients are computed for the thermal distribution of rotational excitations. Although large isotope effects (observed in experiments) are not reproduced here, this level of theory can be used as a foundation for more detailed computational treatment, with accurate information about resonance energies and lifetimes computed and included.

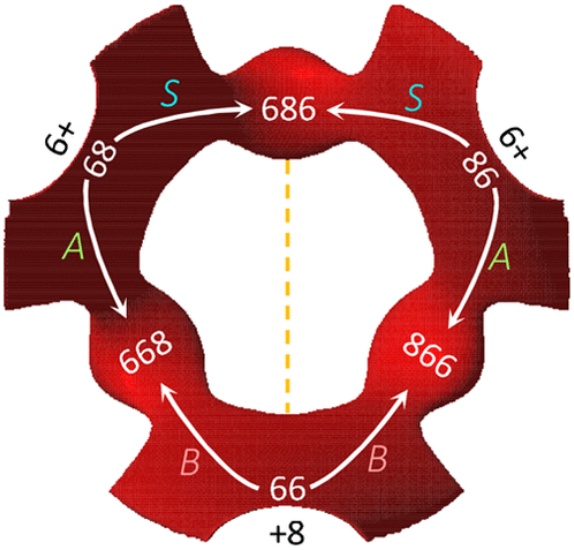

I. Introduction

Ozone in the upper atmosphere of Earth, and in relevant laboratory experiments, is formed by a seemingly simple recombination reaction: $O + O_2 \rightarrow O_3$. One of the mechanisms behind this process involves the formation of the metastable O_3^* and the following stabilization of these intermediate species through energy transfer to the bath gas (the air of the atmosphere—or Ar in the laboratory experiments).[1,2] This energy transfer mechanism, also known as the Lindemann mechanism, is probably responsible for the generation of anomalously large mass-independent fractionation of stable oxygen isotopes,[3–7] which has significant implications for the atmospheric chemistry of the Earth.[8–11] The molecular level origin of this fractionation effect is not entirely understood[12–14] and is a subject of this paper.

In the simplest approach to theoretical description of the ozone forming reaction, one assumes that the metastable intermediate species O_3^* are present in fast equilibrium with reagents (pre-equilibrium approximation):

$$O + O_2 \Leftrightarrow O_3^* + \text{bath gas} \xrightarrow{} O_3 \tag{1}$$

In this case, the rate of ozone formation, written using the equilibrium concentration of O_3^*, leads one to the following expression:

$$\frac{d[O_3]}{dt} = k_{stab}[M][O_3^*] = [M][O][O_2]k_{stab}K \tag{2}$$

where [M] is the concentration of the bath gas. Rate coefficient k_{stab} is introduced for stabilization step, and the equilibrium constant $K = [O_3^*]/[O][O_2]$ is introduced for the formation step. Then, the effective third-order rate coefficient for recombination is simply $k = k_{stab}K$. Statistically, the equilibrium constant K is determined by the ratio of the partition functions of intermediates and reagents, but it also takes into account the activation energy $E^{\ddagger}$ for reaching the intermediate species, thus:

$$k = k_{\mathrm{stab}} e^{-E^{\ddagger}/kT} \; Q_{\mathrm{O}_3^*} / Q_{O+O_2} \tag{3}$$

In principle, when the masses of oxygen atoms are changed by isotopic substitutions, all four moieties in the right-hand side of this expression will change, leading to some isotope effects. So, ideally, a theory is needed that accurately predicts the properties of intermediate ozone states (their spectrum and partition function), their energy relative to reagents, the process of their formation from (and decay back to) the reagents, and, finally, their quenching by the bath gas. At present time such theory does not exist. A brute-force approach for predicting all these properties by rigorous quantum-mechanical calculations remains unfeasible.

During the last two decades a significant body of work was done on several individual pieces of the overall recombination process. Quantum mechanical calculations of energies and lifetimes of O_3^* states were carried out and their possible role in the isotope effects was elucidated.[15–19] Stabilization of the intermediate O_3^* was studied by approximate quantum dynamics methods,[20–27] and using classical trajectories.[28,29] Statistical theory developed by Marcus and co-workers[30–34] helped to rationalize the overall trends of isotopic dependencies. More recently a newer accurate potential energy surface (PES) was developed for ozone,[35] which led to the more complete calculations of the vibrational states of O_3,[36–38] and an improved description of the isotope-exchange process in $\mathrm{O} + \mathrm{O}_2$ collisions.[39–41] Finally, accurate calculations of energies and lifetimes of O_3^* for a broad range of vibrational and rotational excitations was carried out, which allowed to reproduce rather well both temperature and pressure dependencies of the recombination process.[42]

In this paper we apply our recently developed computational tools to improve our understanding of possible isotope effects during the first step of the ozone forming reaction, which is formation and decay of the metastable O_3^*, described in quantum mechanics as scattering resonances. The final step of recombination reaction (stabilization) is treated approximately, by assigning the same value of stabilization cross section to all O_3^* states, irrespectively of their rotational and vibrational content. However, our treatment of O_3^* states is nearly exact. We use the latest PES and employ hyper-spherical coordinates for the description of vibrational and rotational motion of oxygen atoms in ozone. The full range of relevant rotational excitations is included using the Hamiltonian of a "fluid" symmetric top rotor (which is a model appropriate for ozone[14,18]), with its moments of inertia adiabatically adjusted to the instantaneous shape of the vibrating molecule. Large amplitude vibrational motion is described accurately by the symmetry adapted combination of FBR and DVR techniques (for the internal motion and for reaction coordinate, respectively). Efficiency is achieved by sequential diagonalization–truncation procedure. The lifetimes of scattering resonances are computed by the placement of a complex absorbing potential in the asymptotic region of the PES.

Using this accurate approach, we carry out the calculations of O_3^* states (wave functions, energies, lifetimes) for singly and doubly substituted ozone isotopologues, both symmetric and asymmetric isotopomers: $^{16}O^{16}O^{18}O$, $^{16}O^{18}O^{16}O$, $^{16}O^{18}O^{18}O$, and $^{18}O^{16}O^{18}O$. These data are used as input for the kinetic formulas to obtain recombination rate coefficients, and finally to derive and analyze the resultant isotope effects. The tools needed for analysis of isotope effects are also presented, including the definitions of the ΔZPE effect and η-effect, and some review of experimental data, in section II.D and section II.E.

During the course of this work, we realized that it is nearly impossible to rationalize the raw results of our quantum mechanical calculations by, let us say, simply comparing results for one ozone molecule with results for another. Indeed, these calculations, carried out in a broad range of rotational excitations for multiple isotopologues and isotopomers of ozone, produce literally the tens of thousands of bound, resonant and scattering states with widely varying properties. It should also be understood that the isotope effects we are dealing with are not the small regular isotopic shifts familiar from textbooks (that affect fundamentals near the bottom of the potential well). Our focus is on energy range above dissociation threshold, with three-hundred bound vibrational states laying below. At this energy, the spectra of different ozone molecules look completely different and no one-to-one comparison of individual ro-vibrational states is practical.

We also found that if all this swarm of resonance data is routed directly into the kinetics equations (to predict recombination rates), then basically no physical insight emerges. In particular, in this way it is impossible to determine whether there is any sign of the mysterious η-effect in our data, and where this relatively small effect might come from. Indeed, although our results exhibit some features observed in experimental data, the agreement is not yet perfect, and this remaining discrepancy makes it difficult to accept the results of calculations without interpretation. Where the isotope effects are coming from? Are they due to the different number of states in different molecules, or the different decay rates of these states? Or due to the different energies of vibrational states in the spectrum? Or due to the rotational excitation?

In order to answer these and other related questions we found instructive to develop a hierarchy of theory levels, in which our most complete calculations appear at the top. Several lower levels of theory take care of different physical phenomena in the overall process, individually, bringing them into play one by one. Familiar statistical tools, such as partition functions, activation energies and reaction endothermicities, appear in this approach naturally, and are dressed at the very end with quantum mechanical features, such as resonance widths. The isotope effects emerging from each source are thus elucidated and added to the previous level of theory, advancing theoretical treatment and unveiling the complex nature of the isotope effect.

Namely, at what we call the *zeroth-level* of theory all isotopic differences are neglected, including even the mass-dependent effects, and the formula are checked for the correct incorporation of molecular symmetry. This is not trivial, since it requires the inclusion of important factors such as 2 and 1/2 in seven (!) different places in the theory, some of which cancel, but others survive. In the past a lot of confusion was created by including some of these factors in an *ad hoc*way but forgetting some others. Here, in section II.C we report a transparent and complete description of all these factors, which should help other workers to avoid costly mistakes.

At the next level of theory, in section II.F, isotopic masses are introduced, and the resultant isotope effects are analyzed, neglecting the quantum mechanical properties of the reaction coordinate (i.e., neglecting scattering resonances). It is shown that this level of theory, *first-level*, is equivalent to the statistical treatment of the recombination process (such as offered by Marcus and co-workers), except that here we compute the partition functions accurately, in contrast to using approximate analytic models, such as hindered rotor etc. At this level of theory, the emphasis is on how the rotational excitation of the system, determined by two quantum numbers J and Λ, influences two isotope phenomena: ΔZPE-effect (which is named ζ-effect in this work) and η-effect.

The influence of resonance properties on the isotope effects is explored in a separate paper,[48] using two more levels of theory. Namely, at the *second-level* of theory the scattering resonances will be introduced, but will be computed in a simplified way, by neglecting couplings between the diabatic vibrational channels. At the final, *third-level*of theory these couplings will be taken into consideration and the multichannel nature of the ozone forming process will be fully incorporated (see Conclusions).

II. Theory and Methods

II.A. Coordinates, PES and Reaction Pathways

Here we briefly review the properties of the APH hyper-spherical coordinates, and of the ozone PES expressed in these coordinates, since this information is essential for understanding theoretical treatment developed in this paper. More details can be found in our recent papers.[43,44]

Three vibrational degrees of freedom of a triatomic molecule, like ozone, can be described by the APH hyper-spherical coordinates.[45] Although not as intuitive as Jacobi coordinates, hyper-spherical coordinates lead to the simplest form of the ro-vibrational Hamiltonian operator, but also, they permit to take into account molecular symmetry in a rigorous way, and to treat all reaction pathways on equal footing, which is essential for the ozone formation reaction. Recently, these hyper-spherical coordinates were employed for the calculations of the atom exchange in $O + O_2$ collisions,[41] for the predictions of the vibrational spectra of ozone,[37,38] and for the description of its recombination reaction.[42] At a qualitative level ρ, ϑ, and φ describe breathing, bending, and the asymmetric stretching of a triatomic molecule, respectively. As molecule dissociates to the products (or it forms from the reagents) the hyperradius ρ starts playing the role of reaction coordinate: $O_3^* \rightarrow O + O_2$. In the asymptotic range of the PES, the hyper-angles ϑ and φ describe the rotation of O_2 product/reagent relative to the third O atom. Over the years we developed an illustrative way of presenting the PES of ozone in these coordinates using, what we call, the *energy iso-surface* approach.[46] Figure 1a gives a 3D view of the global PES of ozone. In this structure we see three potential energy wells where the stable O_3 molecules are formed. Each well is connected to two dissociation/formation channels through two transition states. These connections are easier to see using the frontal view of the PES, when one looks along the hyperradial direction, as shown in Figure 1b. Energetically and physically equivalent wells (three of them), transition states (six) and entrance/exit channels (three) occur in the case of equivalent oxygen atoms, as, for example, in the $^{16}O^{16}O^{16}O$. However, in the cases of isotopic substitutions they represent physically distinct molecules and their respective formation processes.

Figure 1

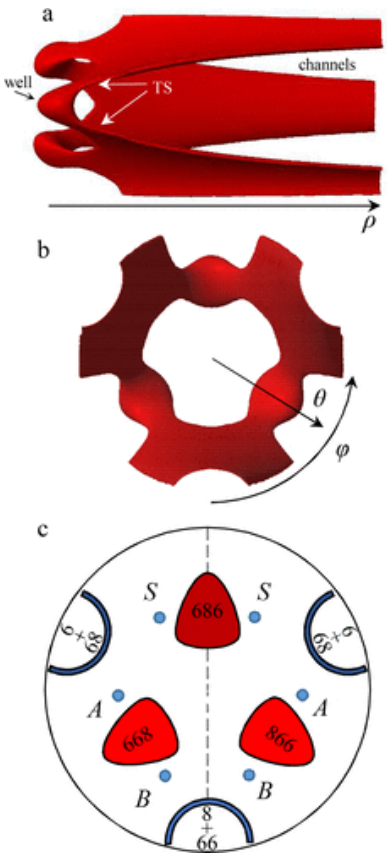

Figure 1. Two upper frames show the side- and the front-views of the PES of O_3 presented as iso-energy surface in hyper-spherical coordinates. Frame a permits one to see, in three dimensions, how the reagent channels connect to the product wells through narrow transition states, as the process of ozone formation proceeds along the reaction path, described here by the hyper-radius ρ. Frame b emphasizes the symmetry of the process described by the hyper-angle φ: three channels, six transition states and three wells. Frame c correlates with frame b, but gives a "map" of possible formation pathways for the case of singly substituted isotopologue, indicating the wells for symmetric $^{16}O^{18}O^{16}O$ and asymmetric $^{16}O^{16}O^{18}O$, the three types of transition states for the processes *A*, *B*, and *S* in eqs 4 and 5, and the two types of the reagent channels, $^{16}O + {}^{18}O^{16}O$ and $^{16}O^{16}O + {}^{18}O$. The dashed line represents the reflection plane of symmetry.

For example, Figure 1c explains the case of single isotopic substitution. One of the wells hosts symmetric isotopomer $^{16}O^{18}O^{16}O$. This well is connected to two physically and energetically equivalent channels:

$$^{16}O + {}^{18}O^{16}O \underset{\leftrightarrow}{S} \{^{16}O^{18}O^{16}O\}^* \underset{\leftrightarrow}{S} {}^{16}O^{18}O + {}^{16}O \quad (4)$$

Two other wells of the PES in Figure 1c hold two asymmetric isotopomers, $^{16}O^{16}O^{18}O$ and $^{18}O^{16}O^{16}O$, that are energetically and physically equivalent. Each such well is connected to two physically distinct entrance channels:

$$^{16}O + {}^{16}O^{18}O \underset{\leftrightarrow}{A} \{^{16}O^{16}O^{18}O\}^* \underset{\leftrightarrow}{B} {}^{16}O^{16}O + {}^{18}O \quad (5)$$

The channel on the left-hand side of this process is effectively deeper, since the zero-point energy of isotopically substituted $^{16}O^{18}O$ is lower than that of the usual $^{16}O^{16}O$ in the right-hand side of the process. We see that,

overall, we have to describe three distinct processes: the formation of symmetric ozone isotopomers, and the formation of asymmetric isotopomers from two different entrance channels. In eqs 4and 5, those are labeled by *S*, *A*, and *B* respectively. Out of six transition states on the PES, two correspond to type *S*, two correspond to type *A* and two correspond to type *B*, as indicated in Figure 1c. Experimental data indicate that the processes of insertion, such as $^{18}O + {}^{16}O^{16}O \rightarrow {}^{16}O^{18}O^{16}O$, are 2 orders of magnitude slower[7] and thus can be ignored.

The picture, similar to Figure 1c, and the formula, similar to eqs 4 and 5, can easily be written for two isotopomers of the doubly substituted ozone:

$$^{18}O + {}^{16}O^{18}O \underset{\leftrightarrow}{\overset{S}{}} \{^{18}O^{16}O^{18}O\}^* \underset{\leftrightarrow}{\overset{S}{}} {}^{18}O^{16}O + {}^{18}O \tag{4'}$$

$$^{18}O + {}^{18}O^{16}O \underset{\leftrightarrow}{\overset{A}{}} \{^{18}O^{18}O^{16}O\}^* \underset{\leftrightarrow}{\overset{B}{}} {}^{18}O^{18}O + {}^{16}O \tag{5'}$$

Compared to the singly substituted case, the difference is that for $^{16}O^{18}O^{18}O$ the deeper formation channel is in the pathway *B* with symmetric diatomic molecule, $^{16}O + {}^{18}O^{18}O$, which has the lowest zero-point energy. In our theory we will always use the deeper entrance channel (first dissociation threshold) as energy reference point, which makes the value of ΔZPE (second dissociation threshold) always positive.

II.B. Kinetics Equations

In contrast to using a continuous density of states (as typically done in statistical theories) we take into account the quantization of the metastable O_3^* states by introducing scattering resonances. For each O_3^* resonance we consider the processes of its formation from, and decay to, two channels of the PES connected to a given well. For example, for each resonance of $\{^{16}O^{16}O^{18}O\}^*$ or $\{^{16}O^{18}O^{18}O\}^*$ we introduce its decay rates into the pathways *A* and *B*, given by two components Γ^A and Γ^B of the resonance width, $\Gamma = \Gamma^A + \Gamma^B$ as follows: $k_{dec}{}^A = \Gamma^A/\hbar$ and $k_{dec}{}^B = \Gamma^B/\hbar$ (everywhere below, Plank's constant is omitted for clarity). For symmetric isotopomers $\{^{16}O^{18}O^{16}O\}^*$ or $\{^{18}O^{16}O^{18}O\}^*$ the two components of the decay rate are exactly equal and physically indistinguishable, so, the total $\Gamma = 2\Gamma^S$ is used. From these (first-order spontaneous) decay rate coefficients the rate coefficients for the formation of each scattering resonance are computed using the equilibrium constant for each pathway: $k_{form}{}^A = K^A\Gamma^A$, $k_{form}{}^B = K^B\Gamma^B$ and $k_{form}{}^S = K^S 2\Gamma^S$. Stabilization and dissociation rate coefficients k_{stab} and k_{diss} are also introduced, and are intentionally taken equal for all resonances, to avoid any bias. Re-excitation of already stabilized O_3 (back to O_3^*) by bath gas collisions, and resonance-to-resonance transitions due to collisions, are ignored.

The analytic treatment of reaction kinetics follows the *steady-state assumption* (just like in the standard Lindemann mechanism) for the concentration of each metastable O_3^* state, independently. Then, the contributions of individual metastable states to the recombination process are determined, similar to eq 2 above, and are added all together, which leads to[17,19,24]

$$\frac{d[O_3]}{dt} = [O^A][O_2^A][M] \sum_{J\Lambda p} \sum_i^{2N} \frac{\Gamma_i^A K_i^A k_{stab}}{\Gamma_i + (k_{stab} + k_{diss}[M])} + [O^B][O_2^B][M] \sum_{J\Lambda p} \sum_i^{2N} \frac{\Gamma_i^B K_i^B k_{stab}}{\Gamma_i + (k_{stab} + k_{diss})[M]} \tag{6}$$

$$\frac{d[O_3^S]}{dt} = [O^A][O_2^A][M] \sum_{J\Lambda p} \sum_i^{N} \frac{2\Gamma_i^S K_i^S k_{stab}}{\Gamma_i + (k_{stab} + k_{diss}[M])} \tag{7}$$

Note that eq 6 for the formation of asymmetric isotopomers, such as $^{16}O^{16}O^{18}O$ or $^{16}O^{18}O^{18}O$, includes two terms for the contributions of two distinct pathways *A* and *B*. The values of reagent concentrations $[O^A]$ and $[O_2{}^A]$,

decay rates Γ_i^A and equilibrium constants K_i^A in pathway *A* are all different than those in pathway *B*: $[O^B]$, $[O_2{}^B]$, Γ_i^B, and K_i^B. Eq 7 for the formation of symmetric isotopomers, such as $^{16}O^{18}O^{16}O$ or $^{18}O^{16}O^{18}O$, looks simpler because those two entrance channels are identical, and the corresponding terms can be combined. In each double-sum of eqs 6–7, the first summation is over the quantum numbers *J* and Λ, and the parity *p*. Note that if the rotational states of positive and negative parities are introduced ($p = \pm$) then Λ is positive only, varied in the range $0 \le \Lambda \le J$, with $0 \le J \le J_{max}$. The second summation in each double-sum of eqs 6 and 7 is over vibrational states, labeled here by *i* (within each set of *J*, Λ, and *p*).

The number of vibrational states of O_3^* is one important factor in eqs 6 vs 7. It is shown in the Appendix that the number of states of asymmetric $^{16}O^{16}O^{18}O$ is expected to be twice larger than the number of states of symmetric $^{16}O^{18}O^{16}O$. This is reflected by $2N$ and N that indicate the upper limits of summation in eqs 6 and 7, respectively. Another factor to consider is equilibrium constant for formation and decay of a resonance. For each individual resonance at energy E_i, the microcanonical equilibrium constant is given by the following expression: $K = (2J + 1)e^{-E_i/kT}/Q_{O+O2}$.[15] The partition function of reagents in the denominator of this expression is affected by isotopic substitutions and, besides a relatively small mass effect, includes also the effect of symmetry. Namely, in the heteronuclear diatomic molecule $^{16}O^{18}O$ of the pathway *A* all rotational states are allowed, while in the homonuclear $^{16}O^{16}O$ (or $^{18}O^{18}O$) of the pathway *B* only odd rotational states are allowed (it is well-known that rotational levels $j = 0, 2, 4$, *etc.*are forbidden).[16,30,38] So, the partition function of reagents for pathway *A* is larger, roughly by a factor of 2, compared to the partition function of reagents in pathway *B*. Note that the formation of symmetric ozone molecules, such as $^{16}O^{18}O^{16}O$ or $^{18}O^{16}O^{18}O$ (labeled by *S*), proceeds through the same entrance channel as pathway *A*, so, the same partition function should be used.

On the basis of this discussion, and from the structure of eqs 6-7, it makes sense to introduce the following three recombination rate coefficients:

$$k^A = \frac{k_{\text{stab}}}{Q^A_{\text{O+O}_2}} \sum_{J\Lambda p} (2J+1) \sum_i^{2N} \mathrm{e}^{-E_i/kT} \frac{\Gamma_i^A}{\Gamma_i + (k_{\text{stab}} + k_{\text{diss}})[\text{M}]} \tag{8}$$

$$k^B = \frac{k_{\text{stab}}}{e^{-\Delta ZPE/kT} Q^B_{\text{O+O}_2}} \sum_{J\Lambda p} (2J+1) \sum_i^{2N} \mathrm{e}^{-E_i/kT} \frac{\Gamma_i^B}{\Gamma_i + (k_{\text{stab}} + k_{\text{diss}})[\text{M}]} \tag{9}$$

$$k^S = \frac{k_{\text{stab}}}{Q^A_{\text{O+O}_2}} \sum_{J\Lambda p} (2J+1) \sum_i^{N} \mathrm{e}^{-E_i/kT} \frac{2\Gamma_i^S}{\Gamma_i + (k_{\text{stab}} + k_{\text{diss}})[\text{M}]} \tag{10}$$

They describe three possible ozone formation processes, consistent with Figure 1c. With these definitions, eqs 6 and 7 turn into a simple intuitive form:

$$\frac{\mathrm{d}[\text{O}_3]}{\mathrm{d}t} = [\text{O}^A][\text{O}_2^A][\text{M}]k^A + [\text{O}^B][\text{O}_2^B][\text{M}]k^B$$

$$\frac{\mathrm{d}[\mathrm{O}_3^S]}{\mathrm{d}t} = [\mathrm{O}^A][\mathrm{O}_2^A][\mathrm{M}]k^S$$

Note that in eq 9 the factor $e^{-\Delta ZPE/kT}$ before the partition function of reagents for pathway *B* is used to account for the zero-point energy difference of O_2 in the entrance channels. As written, these equations are applicable to singly substituted ozone where the entrance channel of pathway *A* is deeper and serves as energy reference. For doubly substituted ozone molecules, where the entrance channel of pathway *B* is deeper, the factor $e^{-\Delta ZPE/kT}$ would appear in the denominator of eq 8, before the partition function of reagents for pathway *A.*

II.C. Zeroth-Level of Theory, and Three Sources of 1/2

First, it is instructive to compare the values of k^A, k^B, and k^S, taking into account symmetry considerations only, since those include relatively important factors, such as 2 and 1/2, that can lead to large effects. Smaller effects due to mass differences are neglected at this stage. We call this the "zeroth" level of theory. At this level we neglect the difference of decay rates into two channels, by setting $\Gamma^A \approx \Gamma^B \approx 1/2\Gamma$ for each resonance. Analysis is simpler in the low-pressure limit, $\Gamma \gg (k_{stab} + k_{diss})[M]$, when the second term in each denominator of eqs 8–10 can be neglected. This gives

$$k^A \approx \frac{k_{\mathrm{stab}}}{\mathrm{O}^{\mathrm{A}}_{\mathrm{O+O_2}}} \frac{1}{2} \sum_{J\Lambda p} (2J+1) \sum_{i}^{2N} \mathrm{e}^{-E_i/kT} \tag{11}$$

$$k_B \approx \frac{k_{\mathrm{stab}}}{e^{-\Delta ZPE/kT}\, \mathrm{Q}^{B}_{\mathrm{O+O_2}}} \frac{1}{2} \sum_{J\Lambda p} (2J+1) \sum_{i}^{2N} \mathrm{e}^{-E_i/kT} \tag{12}$$

$$k^S \approx \frac{k_{\mathrm{stab}}}{\mathrm{O}^{\mathrm{A}}_{\mathrm{O+O_2}}} \frac{1}{2} \sum_{J\Lambda p} (2J+1) \sum_{i}^{N} \mathrm{e}^{-E_i/kT} \tag{13}$$

In order to make these expressions even more concise and thus more transparent, it is convenient to introduce the partition functions of resonances for symmetric and asymmetric ozone molecules as

$$Q_{O_3^*} = \sum_{p} \sum_{i}^{2N} \mathrm{e}^{-E_i/kT} \tag{14}$$

$$Q^S_{O_3^*} = \sum_{p} \sum_{i}^{N} \mathrm{e}^{-E_i/kT} \tag{15}$$

Notice that the $Q_{O3}{}^*$ of asymmetric ozone is expected to be larger than the $Q_{O3}{}^{*S}$ of symmetric ozone by a factor of 2, due to the number of states, $2N$ vs N in eqs 14 and 15. Since the energies E_i of resonances depend on J and

Λ, the values of these partition functions are also rotation-dependent. Using these definitions, the expressions for three rate coefficients reduce to the following:

$$k^A = \frac{1}{2} k_{\text{stab}} \frac{\sum_{J\Lambda}(2J+1)Q_{O_3^*}}{O^{\text{A}}_{O+O_2}} \tag{16}$$

$$k^B = \frac{1}{2} k_{\text{stab}} \frac{\sum_{J\Lambda}(2J+1)Q_{O_3^*}}{e^{-\Delta ZPE/kT}\, O^{\text{B}}_{O+O_2}} \tag{17}$$

$$k^S = k_{\text{stab}} \frac{\sum_{J\Lambda}(2J+1)Q^S_{O_3^*}}{O^{A}_{O+O_2}} \tag{18}$$

Note that besides symmetry related factors, the zero-point energy differences, and the effect of rotational excitation, these formulas look very similar to eq 3 of the Introduction.

Table1 gives a summary of all factors that affect rate coefficients, for these three processes and also for the formation of the usual nonsubstituted ozone $^{16}O^{16}O^{16}O$, included for completeness. The third column of the Table1 is for the splitting of the decay rate Γ onto two pathways. It includes the factor of 1/2 for the formation of asymmetric ozone, since two physically distinct channels, those of pathways *A* and *B*, are available. The fourth column is for the number of O_3^* states. It lists the factor of 1/2 for symmetric ozone molecules. The fifth column is for the number of reagent states in O_2. It lists the factor of 1/2 (in denominator) for those two cases when a homonuclear diatomic molecule is the reagent. Column six of Table1 gives the overall effect, obtained as a product of columns three, four, and five. It shows that we should expect, roughly:

$$2k^A \sim k^B \sim 2k^S \sim k^{666} \tag{19}$$

This nonintuitive result is consistent with eqs 16–18, with experimental data[2–6] and with their interpretation by Janssen et al.[7]

Table 1. Important Factors of 1/2 and Other Symmetry Related Effects for Ozone Forming Reaction

		three sources of 1/2					
process label	isotopic reaction	Γ	$Q_{O3}{}^*$	Q_{O+O2}	resultant rate coefficient	reaction probability (Janssen et al.)	K_{ex}
A	**$^{16}O + {}^{16}O^{18}O \rightarrow {}^{16}O^{16}O^{18}O$**	**1/2**	**1**	**1**	***k*/2**	**×2**	
B	**$^{18}O + {}^{16}O^{16}O \rightarrow {}^{18}O^{16}O^{16}O$**	**1/2**	**1**	$\frac{1}{1/2}$	***k***		**×1/2**
S	**$^{16}O + {}^{18}O^{16}O \rightarrow {}^{16}O^{18}O^{16}O$**	**1**	**1/2**	**1**	***k*/2**	**×2**	
666	**$^{16}O + {}^{16}O^{16}O \rightarrow {}^{16}O^{16}O^{16}O$**	**1**	**1/2**	$\frac{1}{1/2}$	***k***		

Indeed, a careful reading of ref[7] reveals that, in addition to the rate coefficients, experimentalists defined the reaction *probabilities* that are doubled if the reagent is a heteronuclear diatomic (such as in the processes *A* and *S*). This was done, most probably, for convenience, to introduce the quantities that do not differ by a factor of 2, and thus are more straightforward to compare. To emphasize this point, we included fifth column in Table1 that lists these two multiplication factors. Although we do not like the term "reaction probabilities", we will also introduce, for consistency, an equivalent moiety (using Greek kappa symbol), namely: $\kappa^A = 2k^A$, $\kappa^B = k^B$, $\kappa^S = 2k^S$, and $\kappa^{666} = k^{666}$. With these definitions, we should expect that, roughly, $\kappa^A \sim \kappa^B \sim \kappa^S \sim \kappa^{666}$, at the zeroth-level of theory.

II.D. Experimental Data, Isotope effects

The experimental data of Janssen et al. are presented in Figure 2 for the κ^A, κ^B, and $\kappa^S$of singly and doubly substituted ozone. According to their original idea, horizontal axis is chosen to plot the zero-point energy change for the corresponding isotope-exchange process, like in eqs 4 and 5 and in 4′ and 5′. With this choice, the data points for the formation of symmetric isotopomers ($^{16}O + {}^{18}O^{16}O \rightarrow {}^{16}O^{18}O^{16}O$ and $^{18}O + {}^{16}O^{18}O \rightarrow {}^{18}O^{16}O^{18}O$) appear in the middle of the graph, since for these cases ΔZPE is zero. The data points for $^{18}O + {}^{16}O^{16}O \rightarrow {}^{18}O^{16}O^{16}O$ and $^{18}O + {}^{18}O^{16}O \rightarrow {}^{18}O^{18}O^{16}O$ appear on the left side (negative ΔZPE), while the data points for $^{16}O + {}^{18}O^{18}O \rightarrow {}^{16}O^{18}O^{18}O$ and $^{16}O + {}^{16}O^{18}O \rightarrow {}^{16}O^{16}O^{18}O$ appear on the right side (positive ΔZPE). Along the vertical axis we plot the unit-less ratios of rate coefficients, choosing the rate coefficient of symmetric species as a reference (separately for singly and doubly substituted ozone molecules), namely: $R^A = \kappa^A/\kappa^S$, and $R^B = \kappa^B/\kappa^S$. With this choice of reference, $R^S = 1$ by definition, and the corresponding data points appear at the origin of the plot, for both singly and doubly substituted ozone molecules. Note that Janssen et al. used the rate coefficient of $^{16}O + {}^{16}O^{16}O \rightarrow {}^{16}O^{16}O^{16}O$ as a single reference for all other data, which is different from our choice, but just slightly, since the rate coefficients for the formation of all symmetric ozone molecules are quite similar.

Figure 2

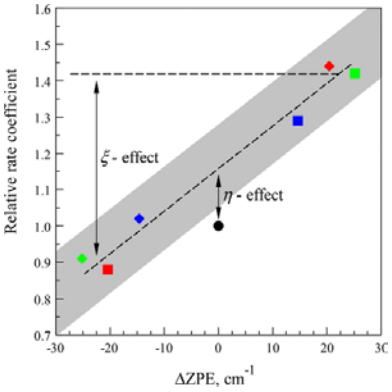

Figure 2. Experimental data of Janssen et al., plotted as explained in the text, for the rates of formation of the symmetric and asymmetric isotopomers of the singly- and doubly substituted isotopologues of ozone. Emphasis is on isotope ^{18}O, but two data points for ^{17}O (blue) are also included. Horizontal axis gives the zero-point energy change of the corresponding atom-exchange reaction (taking into account that in homonuclear diatomics the ground rotational state is $j = 1$). Vertical axis gives rate coefficients (of asymmetric isotopomers) divided by the rate coefficient of symmetric isotopomers. The data for symmetric isotopomers appear at the origin (black symbol). The data for asymmetric isotopomers show large variations and follow a clear trend, called ζ-effect (gray background indicates experimental error bars). The shift of this dependence up from the origin is called *η*-effect. Green and red symbols correspond to $^{16}O^{16}O^{18}O$ and $^{16}O^{18}O^{18}O$, respectively. Squares and diamonds correspond to pathways *A* and *B*, respectively, in eqs 5 and 5′.

Two major effects are seen in Figure 2. One is the ΔZPE trend for the formation of asymmetric isotopomers through pathways *A* and *B*. Larger rate coefficients are measured for processes that enter the PES through deeper channel, which is pathway *A*in the case of singly substituted $^{16}O^{16}O^{18}O$, and pathway *B* in the case of

doubly substituted $^{16}O^{18}O^{18}O$. Experimental data for the single and double substitutions of ^{17}O (not discussed here) also follow this trend, and are included in Figure 2 for completeness. The second effect is the reduction of rate coefficients for the formation of symmetric isotopomers, relative to the ΔZPE-trend of asymmetric isotopomers, the so-called η-effect. In fact, experimental rate coefficients for the formation of all symmetric ozone molecules (including nonsubstituted and triply substituted ozone, and substitutions with isotope ^{17}O), are all relatively close to each other, within 1.5% difference. This is in sharp contrast with wide variations of rate coefficients for asymmetric isotopomers, more than 60%.

On the basis of experimental data in Figure 2, we can introduce two metrics for the isotope effects:

$$\zeta_{\mathrm{exp}} = K^A/K^B \tag{20}$$

$$\eta_{\mathrm{exp}} = (K^A + K^B)/2K^S \tag{21}$$

The first of these will measure ΔZPE-effect (pathways *A* vs *B* for asymmetric isotopomer), while the second will measure η-effect (the average of pathways *A* and *B*for asymmetric isotopomer, vs that of symmetric isotopomer, pathways *S*). Experimental data indicate $\zeta_{exp} = 1.55$ and $\eta_{exp} = 1.16$ for the singly substituted case. For the doubly substituted case, if we want to have $\zeta > 1$, we should flip its definition: $\zeta = \kappa^B/\kappa^A$, since the entrance channel of pathway *B* is deeper in that case. Then, the corresponding experimental data are $\zeta_{exp} = 1.63$ and $\eta_{exp} = 1.16$.

Note that our zeroth-level theory, where all mass effects are neglected and only the symmetry effects are taken into account, predicts $\zeta = 1$ and $\eta = 1$ for both singly and doubly substituted species. This serves as a check for the correctness of the theory (all the factors of 1/2 are correctly included), but also indicates that symmetry considerations alone are insufficient for the explanation of experimentally observed large isotope effects.

II.E. Isotope Enrichments

In this section it is convenient to use “6” for isotope ^{16}O, and “8” for isotope ^{18}O. By definition, isotopic enrichment is

$$\delta = \frac{f_{\mathrm{p}}}{f_{\mathrm{R}}} - 1 \tag{22}$$

where f_R is the fraction of isotope ^{18}O in the *reagents*, which represents natural abundance, while f_P is the ratio of isotopes in the *products*, which is ozone. Doubly substituted isotopologues are extremely rare in the atmosphere, so, we can focus on singly substituted $^{16}O^{16}O^{18}O$ and $^{16}O^{18}O^{16}O$. Heavy isotope is present in each of these molecules, one atom per molecule, so: [8] = 1 × [668] + 1 × [686]. The major isotope ^{16}O is present mostly in the unsubstituted $^{16}O^{16}O^{16}O$, three atoms per molecule, so [6] = 3 × [666]. Thus,

$$f_{\mathrm{p}} \approx \frac{1 \times [668] + 1 \times [686]}{3 \times [666]} \tag{23}$$

Using the third-order kinetics of reactions 6 and 7, this expression transforms as follows:

$$f_{\mathrm{p}} = \frac{1 \times [668] + 1 \times [686]}{3 \times [666]} = \frac{[6][68][M]k^A + [8][66][M]k^B + [6][86][M]k^S}{3[6][66][M]k^{666}} = \frac{1}{3}\frac{[68]}{[66]}\frac{k^A + K_{ex}k^B + k^S}{k^{666}} \tag{24}$$

In the last line of this derivation, we introduced the equilibrium constant for the isotope exchange process 5, defined as

$$K_{\mathrm{ex}} = \frac{[66][8]}{[68][6]} \tag{25}$$

For the reagents, the isotope fraction is

$$f_R \approx \frac{1 \times [68]}{2 \times [66]} = \frac{1}{2}\frac{[68]}{[66]} \tag{26}$$

The substitution of 24 and 26 into 22 gives the final expression for the enrichment:[30,31]

$$\delta = \frac{2}{3}\left(\frac{k^A + K_{ex}k^B + k^S}{k^{666}}\right) - 1. \tag{27}$$

This formula is not particularly transparent, but it can be simplified if we introduce the average rate coefficient for the formation of the asymmetric isotopomer of ozone through two pathways, *A* and *B*:

$$k^{asym} = \frac{k^A + K_{ex}k^B}{2} \tag{28}$$

For the formation of the symmetric isotopomer of ozone we can just rename: $k^{sym} \equiv k^S$. From eq 19, it follows that $k_{\mathrm{rec}}{}^{666} \approx 2k_{\mathrm{rec}}{}^{S}$, based on the zeroth-level of theory (symmetry only), and in agreement with experimental results. Thus, $k_{\mathrm{rec}}{}^{666} \approx 2k^{sym}$. With these definitions:[30,31]

$$\delta = \frac{2}{3}\frac{2k^{asym} + k^{sym}}{2k^{sym}} - 1 = \frac{2}{3}\left(\frac{k^{asym}}{k^{sym}} - 1\right) \tag{29}$$

It appears that the phenomenon of isotope enrichment is driven by the ratio of rate coefficients for the formation of the *asymmetric* and *symmetric* isotopomers of ozone. For asymmetric isotopomers the definition of eq 28 averages over the contributions of the pathways *A* and *B*, so, the difference between the energies of their entrance channels (the ΔZPE difference) does not matter in eq 29, which eliminates the effect of ΔZPE on enrichment δ. But, one can check that, with $K_{\mathrm{ex}} \approx 1/2$:

$$\frac{k^{asym}}{k^{sym}} = \frac{k^A + K_{\mathrm{ex}} k^B}{2k^S} = \eta \tag{30}$$

So, the conclusion is that the enrichment is driven exclusively by the η-effect

$$\delta = \frac{2}{3}(\eta - 1) \tag{31}$$

and appears to be independent of ζ. This interesting property was first demonstrated by Hathorn and Marcus.[30,31] Note that this discussion also gives us an improved definition of η and ζ parameters, as follows:

$$\eta = \frac{k^A + K_{\mathrm{ex}} k^B}{2k^S} \tag{32}$$

$$\zeta = \frac{k^A}{K_{\mathrm{ex}} k^B} \tag{33}$$

More symmetric formula can be obtained if one expresses K_{ex} through K^A and K^B. For example, $\zeta = K^B k^A/(K^A k^B)$.

Equations 32 and 33 are based on the kinetic arguments and take into account the isotope exchange process described by the equilibrium constant K_{ex}. In contrast, definitions we used in the previous section, eqs 20 and 21, were postulated based on the analysis of experimental data in Figure 2. If $K_{ex} \approx 1/2$, the two sets of definitions are consistent. It is important to realize, that the isotope exchange process is 3 orders of magnitude faster than the recombination reaction itself (see ref [7], and references therein), so, the equilibrium $^{16}O + {}^{16}O^{18}O \leftrightarrow {}^{16}O^{16}O + {}^{18}O$ will be readily achieved and should always be taken into account. It should also be stressed that one more factor of 1/2 shows up in the theory due to K_{ex}, and is added to the Table1, accordingly. Thus, one can say that, overall, there are seven factors of 1/2 in the formalism, that take care of symmetry-related effects in the decay rates Γ, the number of metastable O_3^* states, the number of reagent O_2 states, and the isotope exchange process K_{ex} (see Table1).

Using the experimental value of $\eta = 1.16$ (for singly substituted isotopologue we obtain from eq 31 an estimate of enrichment δ = 11%, in good agreement with laboratory measured value close to 13% (see ref [7]and references therein). However, our zeroth-level theory, with $2k^A \sim k^B \sim 2k^S \sim k^{666}$ based on symmetry considerations, gives $\eta = 1$ and δ = 0, which is no enrichment. Thus, symmetry considerations alone can not explain the enrichment of ozone in heavy isotopes.

In the following section, we explore several other sources of isotope effects ζ and η, and the enrichment δ, based on accurate numerical calculations at higher theory levels.

II.F. Mass-Effect, First Level of Theory

The effect of masses in isotopically substituted reactions enters eqs 8–10 through the partition functions of two entrance channels, $Q_{O+O2}{}^A$ and $Q_{O+O2}{}^B$(computed statistically), but also through the energies of scattering resonances E_i. The spectra of E_i are different in different isotopomers and isotopologues, which may lead to an isotope effect. In this subsection we will determine this effect in a somewhat simplified way, without the actual

calculations of energies E_i and decay rates Γ_i of resonances, using the fact that hyper-radius ρ plays the role of reaction coordinate.

The calculation of vibrational states in hyper-spherical coordinates is done sequentially. First, a bound-state problem over hyper-angles θ and ϕ is solved to determine wave functions $\psi_i(\theta,\phi)$ and energies ε_i for the 2D-slices of the PES, at different values of ρ. Figure 3 shows dependencies $\varepsilon_i(\rho)$ computed for singly substituted ozone isotopologue. Asymptotically ($\rho \to \infty$) these curves correlate with the rotational states of O_2reagents/products. In the region of transition state each $\varepsilon_i(\rho)$ curve exhibits a centrifugal barrier, and the property essential for this discussion is that the wave functions of scattering resonances O_3^* are trapped behind these barriers, over the region of covalent well, as shown in Figure 3. The energies E_i, widths Γ_i (decay rates), and wave functions $\Psi_i(\rho,\theta,\phi)$ of these 3D-states are computed at the final, most challenging step of calculations, and normally, all authors proceed straight to that final step. What we propose to do here is to analyze the $\varepsilon_i(\rho)$ dependencies first, since they carry a lot of useful information. Although in the past similar adiabatic curves for ozone have been computed and presented by several authors,[16,18,38] they have never been systematically analyzed, to the best of our knowledge.

Figure 3

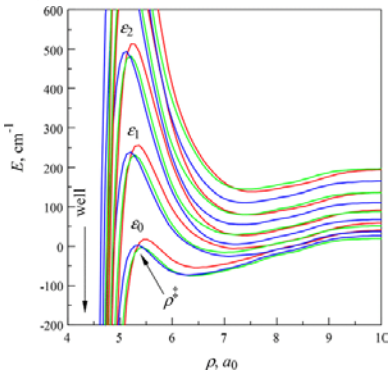

Figure 3. Ro-vibrational energies $\varepsilon_i$computed along the reaction coordinate (hyperradius ρ) for the typical rotational excitation J = 24 and Λ = 2 of the singly substituted isotopologue of ozone. Only one vibrational symmetry is shown, A_1(symmetry B_1 is similar). Transition state region near $\rho^‡$ is emphasized; the potential energy well is also seen. Diabatic curves are color-coded: green, red and blue correspond to the processes *A*, *B* and *S* in eqs 4 and 5, respectively.

Our experience shows that the dominant contribution to the recombination process comes, typically, from one resonance found at energy close to the barrier top.[47] Very narrow resonances, found at energies far below the barrier top, make small contributions because the rates of their formation (by deep tunneling though the barrier) are very low. This suggests an approximation, in which, instead of computing the energies of all resonances, one can assume that for each curve $\varepsilon_i(\rho)$ in Figure 3 there is single resonance at the energy of the barrier top, $E_i = \varepsilon_i(\rho^‡)$. A low-pressure regime is appropriate, since the widths Γ_i of such resonances are not expected to be small. Reaction pathway (*A*, *B*, or *S*) is assigned by comparing each 2D wave function $\psi_i(\theta,\phi)$ computed at $\rho \approx \rho^‡$ to the "map" of the process, that of Figure 1c. This permits us to separate the $\varepsilon_i(\rho)$ curves onto three groups that correspond to pathways *A*, *B*, and *S*, respectively (color-coded in Figure 3). This separation, effectively, splits the 2*N* metastable O_3^* states of asymmetric isotopomer onto two groups, those populated from pathway *A*, and those populated from pathway *B*, with only *N* states in each group:

$$k^A = \frac{k_{stab}}{Q^A_{O+O_2}} \sum_{J\Lambda p} (2J+1) \sum_i^N e^{-\varepsilon_i(\rho^‡)/kT}$$

$$k^B = \frac{k_{stab}}{e^{-\Delta ZPE/kT} Q^B_{O+O_2}} \sum_{J\Lambda p} (2J+1) \sum_i^N e^{-\varepsilon_i(\rho^\ddagger)/kT}$$

$$k^S = \frac{k_{stab}}{Q^A_{O+O_2}} \sum_{J\Lambda p} (2J+1) \sum_i^N e^{-\varepsilon_i(\rho^\ddagger)/kT}$$

Summation over resonances in these expressions has a meaning of partition function at the transition state:

$$Q_{TS} = \sum_p \sum_i^N e^{-(\varepsilon_i - \varepsilon_0)}/kT \tag{34}$$

Note that summation over two parities can be absorbed by the partition function, since the energy of ro-vibrational states does not depend on rotational state parity. Thus, both symmetric and antisymmetric vibrational states (symmetries A_1 and B_1, respectively, see Appendix) are included in Q_{TS}, for each pair of the values of J and Λ. In each pathway, energies can be measured relative to the first resonance (ground state), which now acquires the meaning of activation energy $\varepsilon_0(\rho^\ddagger) = E^\ddagger$, relative to the asymptotic value of energy for each pathway (which means that for pathway B we should set $\varepsilon_0(\rho^\ddagger) = \Delta ZPE + E^\ddagger$, see Figure 4). This gives

$$k^A = \frac{k_{\text{stab}}}{Q^A_{\text{O+O}_2}} \sum_{J\Lambda} (2J+1) \text{e}^{-E^\ddagger_A/kT} Q^A_{\text{TS}} \tag{35}$$

$$k^B = \frac{k_{\text{stab}}}{Q^B_{\text{O+O}_2}} \sum_{J\Lambda} (2J+1) \text{e}^{-E^\ddagger_B/kT} Q^B_{\text{TS}} \tag{36}$$

$$k^S = \frac{k_{\text{stab}}}{Q^A_{\text{O+O}_2}} \sum_{J\Lambda} (2J+1) \text{e}^{-E^\ddagger_B/kT} Q^S_{\text{TS}} \tag{37}$$

Note that the factor $e^{-\Delta ZPE/kT}$ cancels in these equations, which emphasizes the independence of the three reaction pathways at this level of theory. The factor of 2 between the numbers of states in asymmetric and symmetric molecules is still formally achieved, since $Q_{TS}{}^A + Q_{TS}{}^B \approx 2Q_{TS}{}^S$ due to the above-mentioned splitting of $2N$ states.

Figure 4

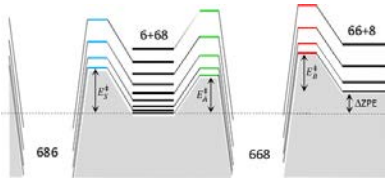

Figure 4. Schematic representation of state energies in two entrance channels, three transition states, and two potential wells for the case of singly substituted ozone isotopologue. The rotational states of $^{16}O^{16}O$ and $^{16}O^{18}O$ in two asymptotic channels are shown by black dashes. The vibrational zero-point energy difference between them is indicated. Lower energy

channel corresponds to $^{16}O^{18}O$ (energy reference, dashed line), which also has twice more states than the usual $^{16}O^{16}O$. Colored dashes indicate quantum states at three transition states: green, red and blue for the processes *A*, *B*, and *S* in eqs 4 and 5, respectively. Their corresponding activation energies are indicated. The connections of these states to two wells, hosting symmetric $^{16}O^{18}O^{16}O$ and asymmetric $^{16}O^{16}O^{18}O$ isotopomers, are shown by thin lines. This schematic covers (roughly) one-half of the diagram in Figure 1c.

The moieties $E^{\ddagger}$ and Q_{TS} that appear eqs 35–37, are also found in statistical approach to the recombination rate, so, one can argue that this level of theory is equivalent to the statistical approach. However, in the practical application of statistical theory the position, energy, and partition function of the transition state are determined approximately, using analytic models such as hindered rotor. Here we accurately compute $E_A^{\ddagger}$, $E_B^{\ddagger}$, $E_S^{\ddagger}$, Q_{TS}^{A}, Q_{TS}^{B}, and Q_{TS}^{S}, and analyze the resultant isotope effects.

At this level of theory, according to eqs 32 and 33, and using $\mathrm{K_{ex}} = \mathrm{e}^{-\Delta \mathrm{ZPE/kT}} \mathrm{Q^{B}_{O+O_2}/Q^{A}_{O+O_2}}$:

$$\zeta = \frac{1}{\mathrm{e}^{-\Delta \mathrm{ZPE/kT}}} \times \frac{\sum_{J\Lambda}(2J+1)\mathrm{e}^{-E_A^{\ddagger}/kT} Q_{TS}^{A}}{\sum_{J\Lambda}(2J+1)\mathrm{e}^{-E_B^{\ddagger}/kT} Q_{TS}^{B}} \tag{38}$$

$$\eta = \frac{\sum_{J\Lambda}(2J+1)\left(e^{-E_A^{\ddagger}/kT} Q_{TS}^{A} + \mathrm{e}^{-E_B^{\ddagger}/kT} Q_{TS}^{B} \mathrm{e}^{-\Delta \mathrm{ZPE/kT}}\right)}{2\sum_{J\Lambda}(2J+1)\mathrm{e}^{-E_S^{\ddagger}/kT} Q_{TS}^{S}} \tag{39}$$

Note that these expressions include only the properties of three transition states *A*, *B*, and *S*. The partition functions of reagents in the asymptotic channels cancel completely. One can also define, compute and analyze the "local" values of ζ and η for each pair of *J* and Λ:

$$\zeta_{J\Lambda} = \frac{1}{\mathrm{e}^{-\Delta \mathrm{ZPE}/\mathrm{kT}}} \times \mathrm{e}^{-\left(E_A^{\ddagger} - E_B^{\ddagger}\right)/kT} \frac{Q_{TS}^{A}}{Q_{TS}^{B}} \tag{40}$$

$$\eta_{J\Lambda} = \frac{1}{2}\left(\mathrm{e}^{-\left(E_A^{\ddagger} - E_S^{\ddagger}\right)/kT} \frac{Q_{TS}^{A}}{Q_{TS}^{S}} + \mathrm{e}^{-\left(E_B^{\ddagger} - E_S^{\ddagger}\right)/kT} \frac{Q_{TS}^{B}}{Q_{TS}^{S}} \mathrm{e}^{-\Delta \mathrm{ZPE}/\mathrm{kT}}\right) \tag{41}$$

These last two equations give the contribution of each term in the sums of eqs 38 and 39 and permit to monitor the role of rotational excitation in isotope effects. Figure 4 emphasizes the meaning of, and connections between ΔZPE, $E_A^{\ddagger}$, $E_B^{\ddagger}$, $E_S^{\ddagger}$, Q_{TS}^{A}, Q_{TS}^{B}, and Q_{TS}^{S}.

III. Results

Overall, eqs 40 and 41 contain six ratios that one may want to explore separately: Q_{TS}^{A}/Q_{TS}^{B}, Q_{TS}^{A}/Q_{TS}^{S}, Q_{TS}^{B}/Q_{TS}^{S}, $\mathrm{e}^{-(E_A^{\ddagger} - E_B^{\ddagger})/kT}$, $\mathrm{e}^{-(E_A^{\ddagger} - E_S^{\ddagger})/kT}$, and $\mathrm{e}^{-(E_B^{\ddagger} - E_S^{\ddagger})/kT}$. For each of these factors, we computed its dependence on the two quantum numbers of rotational excitation, J and Λ, for the cases of the singly and doubly substituted isotopologues of ozone. All those data are available to readers in the Supporting Information. As for absolute values, at room temperature all partition functions are ~1.4 for the vibrational states of each symmetry, A_1 and B_1 that (combined with the rotational states of proper parities) must be added together in eq 37. So, on average, the process of ozone formation includes less than three ($Q_{TS} = \sum_{\rho} \approx 2.8$) vibrational states of O_3^* per each rotational state characterized by J and Λ. As for the ratios Q_{TS}^{A}/Q_{TS}^{B}, Q_{TS}^{A}/Q_{TS}^{S}, and Q_{TS}^{B}/Q_{TS}^{S}, they all stay very close to one, through the entire range of relevant rotational excitations $J$and Λ. First conclusion here is that virtually no isotope effects come from the difference in the number of states at the barrier region in the three pathways of ozone formation: *A*, *B*, and *S*.

This result permits us to come out with a useful approximation to eqs 40 and 41:

$$\zeta_{J\Lambda} = \mathrm{e}^{-\left(E_A^{\ddagger} - E_B^{\ddagger}\right)/kT} / \mathrm{e}^{-\Delta \mathrm{ZPE}/\mathrm{kT}} \tag{42}$$

$$\eta_{J\Lambda} = \left(\mathrm{e}^{-\left(E_A^{\ddagger} - E_S^{\ddagger}\right)/kT} + \mathrm{e}^{-\left(E_B^{\ddagger} - E_S^{\ddagger}\right)/kT} \mathrm{e}^{-\Delta \mathrm{ZPE}/\mathrm{kT}}\right)/2. \tag{43}$$

Each $E^{\ddagger}$ includes three contributions: the potential energy, the rotational energy, and the vibrational zero-point energy (all at the transition state point $\rho^{\ddagger}$). The effect of potential energy largely cancels, since the transition state points for pathways *A*, *B* and *S* occur at roughly the same value of ρ. When there is no overall rotation (J = 0), the effect can only come from the differences of the vibrational zero-point energies at the transition state, which we will denote $\Delta \mathrm{ZPE}^{\ddagger}$. So, we end up with a very simple and useful formula:

$$\zeta_{J=0} = \mathrm{e}^{+\Delta \mathrm{ZPE}^{\ddagger}/\mathrm{kT}} \tag{44}$$

Although the local vibrational zero-point energy does change along the reaction path ρ, one may assume that it correlates with the vibrational zero-point energy of O_2 in the asymptotic region, which is ΔZPE. At room temperature ($kT \sim 200$ cm^{-1}) and using ΔZPE ~ 20 cm^{-1}, one can readily make a simple estimate of the isotope effect due to ΔZPE: $\zeta_{J=0} \sim e^{0.1} \sim 1.10$, for the nonrotating ozone molecule.

This simple estimate gives the right direction of the isotope effect, but the magnitude deviates from the accurately computed value (see below), simply because $\Delta ZPE^{\ddagger}$ at the transition state is not really equal to the asymptotic ΔZPE of O_2. In order to obtain a better estimate, we tried to derive a more accurate value of $\Delta ZPE^{\ddagger}$using two alternative methods. In one approach we simply computed the $\varepsilon_i(\rho)$ curves for nonrotating ozone molecule, $J = 0$, when there is no rotational excitation, so that the difference of $\varepsilon_0(\rho^{\ddagger})$ at two transition states gives vibrational contribution directly, $\Delta ZPE^{\ddagger}$. In an alternative method, we analyzed the spectrum of $\varepsilon_i(\rho^{\ddagger})$ which has two local modes that are normal to the reaction coordinate ρ. We found the first excited state of each mode, determined its frequency, and computed the vibrational zero-point energy from those (all done for typical rotational excitation $J = 24$ and $\Lambda = 2$). Importantly, the results of two methods were very similar to each other, giving $\Delta ZPE^{\ddagger} \sim 32$ cm^{-1} for both singly- and doubly- substituted isotopologues (see Supporting Information). With this value, the estimate of vibrational contribution to ζ-effect is $\zeta_{J=0} \sim 1.18$, considerably larger than the estimate of the previous paragraph.

In Figure 5, the dependencies of $\zeta_{J\Lambda}$ on *J*and Λ, accurately computed using eq 40, are presented for singly and doubly substituted isotopologues. We can see that, indeed, in the range of smaller rotational excitations the value of $\zeta_{J\Lambda}$ tends toward $\zeta_{J=0} \sim 1.18$ predicted by the approximate eq 44. More specifically, the value of $\zeta_{J\Lambda} = 1.22$ is found to be around $J = 16$ and $\Lambda = 13$. However, as the rotational excitation increases, the value of $\zeta_{J\Lambda}$ decreases. For example, near $J = 48$ and $\Lambda = 0$, it is reduced to $\zeta_{J\Lambda} \approx 1$, which means that the rotational excitation acts against the vibrational ΔZPE difference, compensating for it and reducing the resultant ζ-effect. Summation over *J* and Λ in eq 38 gives us $\zeta = 1.126$ and 1.127, for singly and doubly substituted isotopologues, respectively, which is smaller isotope effect compared to the $J = 0$ case. Our conclusion here is that this level of theory, equivalent to the statistical treatment of the recombination process, is insufficient to explain the large magnitude of ζ-effect observed in the experiments ($\zeta_{exp} = 1.55$ and 1.63).

Figure 5

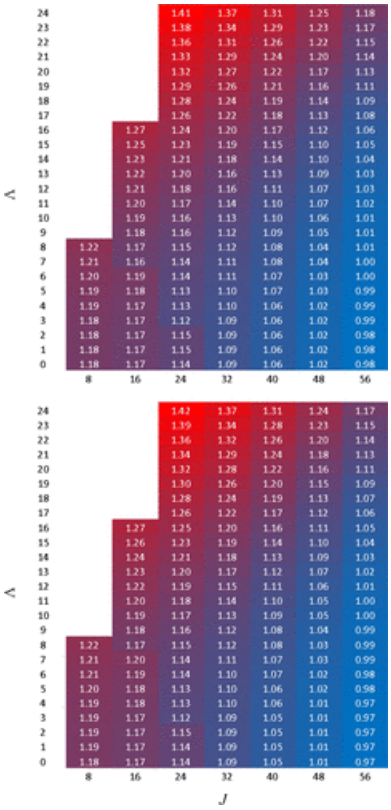

Figure 5. Accurately computed dependence of ζ-effect on the two quantum numbers of rotational excitation, J and Λ, plotted along horizontal and vertical axes, respectively. The first level of theory is used to include mass-effect on vibrational and rotational excitations. Upper and lower frames are for singly and doubly substituted isotopologues, respectively. As $J \rightarrow 0$ the value of ζ approaches 1.18, consistent with estimate based on the vibrational ZPE only. In the range of large $J \sim 50$ the value of ζ approaches 1, indicating that rotational excitation equalizes the deeper and shallower reaction channels, acting against the ZPE difference. Only in the range of extreme rotational excitations (unphysically large Λ) is the value of ζ predicted to be large.

In Figure 6 the dependencies of $\eta_{J\Lambda}$ on $J$and Λ are presented for singly- and doubly substituted isotopologues. We immediately see that the behavior of $\eta_{J\Lambda}$ is different for singly and doubly substituted isotopologues. This already means that the dependencies we observe here are very unlikely to explain experimental η-effect, simply because in the experiment η-effect is the same for singly and doubly substituted isotopologues (namely, asymmetric isotopomers are always favored). Interestingly, we see again that the values of $\eta_{J\Lambda}$ change rather drastically when we change J and Λ. For example, if we change the rotational excitation from $J = 16$, $\Lambda = 13$ to $J = 48$, $\Lambda = 0$ the value of $\eta_{J\Lambda}$ evolves from $\eta_{J\Lambda} = 0.86$ to 1.17 for singly substituted isotopologue, and from $\eta_{J\Lambda} = 1.18$ to 0.86 for doubly substituted isotopologue. However, when we compute the overall effect, by summation over J and Λ in eq 39, these contributions, again, compensate each other, leading to the relatively small values of the overall isotope effect: $\eta = 0.954$ and 1.036 for singly and doubly substituted isotopologues, respectively. Not only are these values small (compared to the experimental value of $\eta_{exp} = 1.16$) but also they deviate from 1.000 in two opposite directions. Thus, again, our conclusion is that this level of theory, equivalent to the statistical treatment of the recombination process, is insufficient to explain η-effect and does not help to determine its origin.

Figure 6

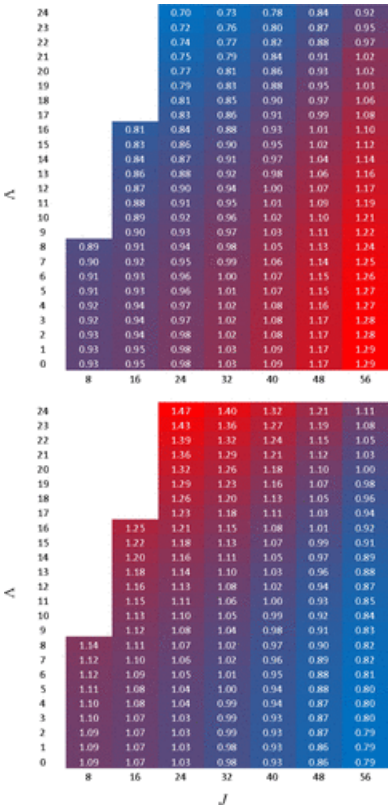

Figure 6. Accurately computed dependence of η-effect on the two quantum numbers of rotational excitation, J and Λ, plotted along horizontal and vertical axes, respectively. The first level of theory is used to include mass-effect on vibrational and rotational excitations. In contrast with Figure 5, these dependencies are opposite for singly and doubly substituted isotopologues, shown in the upper and lower frames, respectively. In the range of typical rotational excitations, $25 < J < 40$ and $\Lambda < 8$, the value of η deviates from 1 by a few percent only.

Rather strong dependencies of $\zeta_{J\Lambda}$ and $\eta_{J\Lambda}$on J and Λ (Figures 5 and 6) are explained by the effect of masses on the rotational energy of O_3^* complex at the transition state, $E^{\ddagger}$. To build an alternative and even more transparent model one can use an approximate rotational Hamiltonian in Jacobi coordinates (at the transition state):

$$E_{\rm rot} = \frac{J(J+1)}{2\mu_{\rm O+O_2}R^2} + \frac{\Lambda^2}{2\mu_{\rm O_2}r^2} \tag{45}$$

to describe the effect of rotation on the energy of the centrifugal barrier. Again, we can use $E^{\ddagger} = V_{\rm pot} + E_{\rm rot} + ZPE_{\rm vib}$ (minus ΔZPE for the upper channel, see Figure 4). Here the reduced masses of O_2 and O + $O_2$are specific to pathways *A* and *B*. Parameters for the pathway *S* are the same as for pathway *A* (see Figure 1c). The substitution of these equations in eqs 42 and 43 gives

$$\zeta_{J\Lambda} \approx e^{-\Delta E_{\rm rot}/kT}\zeta_{J=0} \tag{46}$$

$$\eta_{J\Lambda} \approx \left(1 + \zeta_{J\Lambda}{}^{-1}\right)/2 \tag{47}$$

where $\Delta E_{rot} = E_{rot}{}^{A} - E_{rot}{}^{B}$ (for the singly substituted isotopologue) and $\zeta_{J=0}$ is given by eq 44. For the doubly substituted isotopologue one should define $\Delta E_{rot} = E_{rot}{}^{B} - E_{rot}{}^{A}$, consistent with the discussion of eq 20 above. We found that the trends predicted by these simple formulas are in reasonable semiquantitative agreement with accurately computed results presented in Figures 5 and 6, which confirms one more time that the effect of masses on the vibrational and rotational energies of transition states in ozone cannot explain large isotope effects seen in the experiments.

Finally, the absolute values of the recombination rate coefficients depend on stabilization rate coefficients k_{stab} in eqs 35–37, that in turn depend on stabilization cross sections. Accurate calculations of stabilization cross sections go beyond the scope of this paper. A constant value of $\sigma_{stab} = 154\ a_0{}^2$ was adopted from ref (25). Using this value, we computed the contributions of different rotational excitations, J and Λ, into the rate coefficients or recombination k^A, k^B, and k^S. Because of space considerations those data are presented in the Supporting Information, for singly and doubly substituted isotopologues. The practically useful information is the range of J and Λ values that make significant contributions to the recombination process. We found that at this level of theory, the largest contributions come from a "stripe" that extends between J= 16, Λ = 13 and J = 48, Λ = 0. The range of J and Λ values considered here is broader, and thus, it is well sufficient for a converged description of the recombination process.

IV. Conclusions

In this paper, we presented in sufficient detail the most important components of the theory for the description of the isotope effects in the recombination reaction that forms ozone, including the introduction of three reaction pathways for symmetric and asymmetric isotopomers, a brief review of relevant experimental data for singly- and doubly substituted isotopologues, the definitions of ζ-effect and η-effect, and the introduction of isotopic enrichment δ. The two levels of theory are presented to elucidate the role of molecular symmetry and atomic masses in the recombination process.

The issue of symmetry is not trivial, since important factors, such as 1/2 and 2, appear in seven different places in the formalism. This question has never been presented in the literature in sufficient detail, which created significant confusion in the past. The literature has examples when a missing factor of 1/2 was interpreted as a source of an isotope effect, and other examples when the missing factor was introduced in an *ad hoc* way to reproduce experimental results but based on a wrong argument. Now we have a transparent summary of all these symmetry-related factors, collected in one table, and accounted for in a consistent and rigorous way in the theory of recombination rate. We showed that if all these effects are taken into account properly, then no anomalous isotope effects emerge. We call this zeroth-level theory, to emphasize the fundamental importance of molecular symmetry, as a basis for other more detailed levels of description.

At the next level of theory developed in this paper, we explored in detail the effect of the masses of oxygen isotopes, including the vibrational and rotational components of molecular excitations in a broad range. For this treatment to be transparent, we employed an approximation, by allowing only one resonance per rotational–vibrational channel, chosen right at the top of centrifugal barrier. This approximation is expected to represent, on average, the spectrum of scattering resonances in a real molecule, since only the resonances close to barrier top (slightly below or slightly above it) are known to make significant contributions to the recombination process, and typically there is only one such resonance per rotational–vibrational channel, simply due to the quantization of vibrational motion. It came as a surprise for us that the formulas we obtained in this case are

basically equivalent to the statistical treatment of the recombination process, where transition state is quantized, and the corresponding partition function is introduced.

At this first level of theory, we found that barely any isotope effect come from the number of vibrational states participating in the three pathways of ozone formation: *A*, *B*, and *S*. The ratios of the corresponding partition functions are all close to one, and this holds at any level of the rotational excitation. Isotope effects come from the differences of transition state energies in three pathways. Vibrational contribution to this energy, known as the ΔZPE effect, can account for about 18% difference in the formation rates of two pathways, *A* and *B*, but only if the molecule does not rotate. As rotational excitation increases, the centrifugal energy of the deeper channel (pathway *A* in the singly substituted and pathway *B* in the doubly substituted case) grows faster. So, rotational excitation acts *against* the vibrational ΔZPE, reducing the resultant ζ-effect. At the high level of the rotational excitation, near $J = 50$, rotational energy becomes sufficient to compensate the difference in the vibrational zero-point energies, so, the two transition state energies become equal and ζ-effect disappears completely. When we sum over rotational states (at room temperature) the average ζ-effect is only 13%, which can not explain the ∼60% difference of rates for pathways *A* and *B* observed in the experiment.

A similar phenomenon is found in our calculations for the *η*-effect. Although the extreme rotational excitations, such as very large *J* values, or very large Λ values, lead to a rather significant difference between symmetric and asymmetric isotopomers, these effects are local and mutually cancel when we average over the distribution of *J*and Λ (at room temperature). Moreover, local *η*-effects we see in our calculations occur in opposite directions for singly and doubly substituted isotopologues (with the rotationally averaged values of +4% and −4%), in contrast to experimental measurements that show the same direction and magnitude of η-effects for all ozone molecules, about +16%. This indicates that the statistical description of mass-effects can not give the explanation of the mysterious *η*-effect observed in experiments.

These two levels of theory provide a solid foundation for more rigorous theoretical treatment reported elsewhere,[48] that includes finer components such as accurately computed resonance energies, lifetimes, and channel-to-channel couplings.

Appendix

Symmetry Considerations

The number of vibrational states is an important factor in eqs 6 and 7. Here we consider isotopes ^{16}O and ^{18}O only, both of which are spin-less bosons. The vibrational wave functions of scattering resonances O_3^* are localized over the covalent well, where the electronic wave function of the system is symmetric, X^1A_1. This means that the ro-vibrational wave functions of the molecule should also be symmetric. The detailed analysis of symmetry for the ro-vibrational states of ozone was presented in a recent dissertation.[49] Here we focus on singly- and doubly-substituted ozone molecules, described using C_{2v} point group, with the *z*-axis, used to define quantum number Λ and positioned in the plane of the molecule, along the principal axis of inertia with the smallest component of the moment of inertia. (An alternative approach would be to use, following Bunker,[50] the permutation-inversion symmetry group, as it was done in a recent paper.[38]) The symmetry of rotational states is determined by parity, but differently for the even and odd values of Λ, which, in turn, sets symmetry restrictions on vibrational states (see ref[49] for details). It is demonstrated that for the *even* values of Λ the rotational states of *positive* and *negative* parities can only be combined with the vibrational states of symmetries A_1 and B_1, respectively. But for the *odd* values of Λ this is just opposite: *negative* and *positive* parities are combined with vibrational symmetries A_1 and B_1, respectively. In the Fig. 1c of the PES the vibrational wave functions of symmetry A_1would be symmetric, while those of symmetry B_1 would be antisymmetric with respect

to the sign change of the hyper-angle ϕ (or, equivalently, with respect to reflection through the symmetry plane). This is also emphasized in the Fig. 7 of this Appendix.

Figure 7

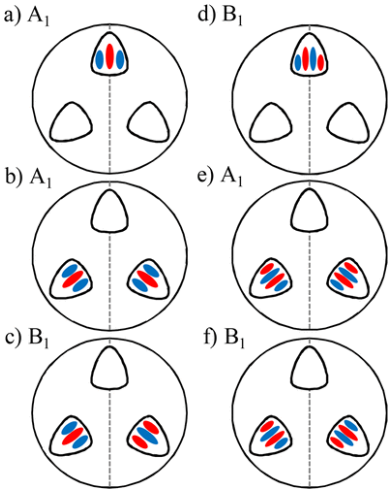

Figure 7. Frames a–c represent, schematically, the structure of the wave functions of three nearly degenerate states with two quanta of excitation. Frame a shows the state of symmetric isotopomer $^{16}O^{18}O^{16}O$, whereas frames b and c show the two possible states of asymmetric isotopomer $^{16}O^{16}O^{18}O$. Frames d–f represent the same information for the next vibrational state, with three quanta of excitation. State symmetries are indicated in each case.

Strictly speaking, this means that only 50% of the vibrational states are allowed (compared to the case with no symmetry, such as $^{16}O^{17}O^{18}O$, where each vibrational state could be combined with two rotational states, of both parities). But in practice no vibrational states are disregarded, simply because the parity of the rotational wave functions does not affect the centrifugal potential, determined solely by Λ (and *J*). Namely, for any given values of *J* and Λ, the calculations of vibrational states are carried out to determine both symmetric (A_1) and antisymmetric (B_1) states. Each computed vibrational state is assumed to be combined with the rotational state of correct parity according to the rule outlined above, depending on whether Λ is even or odd. So, both vibrational symmetries, A_1 and B_1, are retained in the spectrum. The only exception to this, is the case of Λ = 0 (any *J*) where only the positive parity of rotational state is possible and thus only symmetric vibrational states (A_1) are allowed. Antisymmetric vibrational states (B_1) should be disregarded for all Λ = 0 cases.

Importantly, this selection rule applies to both symmetric and asymmetric ozone molecules, and, by itself, does not seem to cause any difference in the number of states in symmetric and asymmetric isotopomers, such as in $^{16}O^{18}O^{16}O$ *vs* $^{16}O^{16}O^{18}O$. What happens to be important, is the presence of two equivalent wells for the case of $^{16}O^{16}O^{18}O$, *vs* only one well in the case of $^{16}O^{18}O^{16}O$. To understand this, consider a finite energy range, which contains two consecutive vibrational states of the asymmetric stretching progression, with say two and three quanta of excitation along the hyper-angle ϕ: ψ_2 and ψ_3. It follows from Figure 1c and Figure 7 that since the well of symmetric $^{16}O^{18}O^{16}O$ is crossed by the symmetry plane, the wave function of ψ_2 is symmetric (A_1) while the wave function of ψ_3 is anti-symmetric (B_1). Combined with the rotational states of proper parities these excitations will give *two* ro-vibrational states of $^{16}O^{18}O^{16}O$ in the considered energy range. Now consider the same two vibrational excitations in the case of asymmetric $^{16}O^{16}O^{18}O$. From Figure 7, we understand that since symmetry plane passes between the two wells, the symmetry of vibrational wave functions is not determined by the number of excitation quanta in each well, but rather by how the wave functions of the two wells are combined to form a global state. On the basis of a textbook double-well problem, we expect to see in the spectrum a pair of nearly degenerate states for each level of vibrational excitation: $(\psi_2^L \pm \psi_2^R)/\sqrt{2}$ and $(\psi_3^L \pm \psi_3^R)/\sqrt{2}$, where indexes *L* and *R* label the wave functions in the right and left wells of $^{16}O^{16}O^{18}O$ in Fig. 7. Within each pair, one state, obtained by "in-phase" superposition, is symmetric (A_1) while the other, obtained by "out-

of-phase" superposition, is antisymmetric (B_1). Being combined with the rotational states of proper parities, they would give *four* ro-vibrational states in the energy range chosen for this example (see Figure 8).

Figure 8

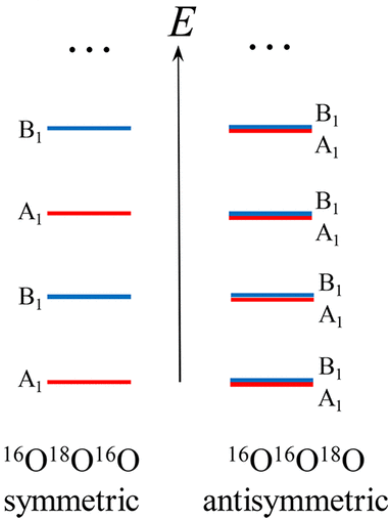

Figure 8. Schematic representation of the vibrational spectrum of the symmetric and asymmetric isotopomers of ozone, $^{16}O^{18}O^{16}O$ and $^{16}O^{16}O^{18}O$, based on symmetry considerations presented in Figure 7. In symmetric ozone (left), the states of two symmetries intercalate in the spectrum, since symmetry is determined by the number of excitation quanta (A_1 for the even numbers of excitations, and B_1 for the odd). In asymmetric ozone, the states of both symmetries occur at every energy, due to the double-well nature of wave functions. This means that the asymmetric isotopomers of ozone have twice as many states, compared to symmetric isotopomers.

The bottom line of this discussion is that on the global PES of ozone, such as presented in Figure 1c and Figure 7, the number of states of asymmetric $^{16}O^{16}O^{18}O$, 2*N*, is roughly twice as large as the number of states of symmetric $^{16}O^{18}O^{16}O$, *N*. Deviations from the perfect factor of 2 can occur due to the mass effect and due to larger coupling between the wells at higher energies (non-negligible splitting). We checked and found, by the accurate calculations of vibrational states, that for the bound states below dissociation threshold the ratio is, indeed, very close to two. A molecule with no symmetry, such as $^{16}O^{17}O^{18}O$, would have twice as many states than the C_{2v} molecules, namely: 2*N*states per each of the three wells in Figure 1c ($^{16}O^{17}O^{18}O$, $^{17}O^{16}O^{18}O$ and $^{16}O^{18}O^{17}O$) or 6*N* states in the entire configuration space, again, just because each vibrational state would be allowed to combine with the rotational states of both parities.

Acknowledgments

This research was supported by the NSF Atmospheric Chemistry Program, Division of Atmospheric Sciences, Grant No. AGS-1252486. This research used the resources of the National Energy Research Scientific Computing Center, which is supported by the Office of Science of the U.S. Department of Energy under Contract No. DE-AC02-05CH11231.

References

1 Luther, K.; Oum, K.; Troe, J. The role of the radical-complex mechanism in the ozone recombination/dissociation reaction. *Phys. Chem. Chem. Phys.* 2005, *7*, 2764– 2770, DOI: 10.1039/b504178c

2 Guenther, J.; Krankowsky, D.; Mauersberger, K.Third-body dependence of rate coefficients for ozone formation in ^{16}O–^{18}O mixtures. *Chem. Phys. Lett.*2000, *324*, 31– 36, DOI: 10.1016/S0009-2614(00)00550-9

3 Krankowsky, D.; Mauersberger, K. Heavy ozone - a difficult puzzle to solve. *Science* 1996, *274*, 1324–1325, DOI: 10.1126/science.274.5291.1324

4 Anderson, S. M.; Hulsebusch, D.; Mauersberger, K.Surprising rate coefficients for four isotopic variants of O + O_2 + M. *J. Chem. Phys.* 1997, *107*, 5385– 5392,DOI: 10.1063/1.474247

5 Janssen, C.; Guenther, J.; Krankowsky, D.;Mauersberger, K. Relative formation rates of $^{50}O_3$ and $^{52}O_3$ in $^{16}O/^{18}O$ mixtures. *J. Chem. Phys.* 1999, *111*,7179– 7182, DOI: 10.1063/1.480045

6 Mauersberger, K.; Erbacher, B.; Krankowsky, D.;Gunther, J.; Nickel, R. Ozone isotope enrichment: Isotopomer-specific rate coefficients. *Science* 1999,*283*, 370– 372, DOI: 10.1126/science.283.5400.370

7 Janssen, C.; Guenther, J.; Mauersberger, K.;Krankowsky, D. Kinetic origin of the ozone isotope effect: a critical analysis of enrichments and rate coefficients. *Phys. Chem. Chem. Phys.* 2001, *3*, 4718–4721, DOI: 10.1039/b107171h . See also: Tuzson, B. *Symmetry Specific Study of Ozone Isotopomer Formation*. Ph.D. Dissertation, University of Heidelberg: 2005.

8 Thiemens, M. H. Mass-independent isotope effects in planetary atmospheres and the early solar system. *Science* 1999, *283*, 341– 345, DOI: 10.1126/science.283.5400.341

9 Thiemens, M. H. Nonmass-Dependent Isotopic Fractionation Processes: Mechanisms and Recent Observations in Terrestrial and Extraterrestrial Environments. *Treatise on Geochemistry* 2007, *4*, 1–24, DOI: 10.1016/B0-08-043751-6/04037-8

10 Thiemens, M. H. History and applications of mass-independent isotope effects. *Annu. Rev. Earth Planet. Sci.* 2006, *34*, 217– 262, DOI: 10.1146/annurev.earth.34.031405.125026

11 Thiemens, M.; Chakraborty, S.; Dominguez, G.The physical chemistry of mass-independent isotope effects and their observation in nature. *Annu. Rev. Phys. Chem.* 2012, *63*, 155– 177, DOI: 10.1146/annurev-physchem-032511-143657

12 Mauersberger, K.; Krankowsky, D.; Janssen, C.;Schinke, R. Assessment of the ozone isotope effect.*Adv. At., Mol., Opt. Phys.* 2005, *50*, 1– 54, DOI: 10.1016/S1049-250X(05)80006-0

13 Schinke, R.; Grebenshchikov, S. Y.; Ivanov, M. V.;Fleurat-Lessard, P. Dynamical studies of the ozone isotope effect: A status report. *Annu. Rev. Phys. Chem.* 2006, *57*, 625– 661, DOI: 10.1146/annurev.physchem.57.032905.104542

14 Kryvohuz, M.; Marcus, R. A. Coriolis coupling as a source of non-RRKM effects in ozone molecule: Lifetime statistics of vibrationally excited ozone molecules. *J. Chem. Phys.* 2010, *132*, 224305–224314, DOI: 10.1063/1.3430514

15 Babikov, D.; Kendrick, B. K.; Walker, R. B.; T Pack, R.; Fleurat-Lesard, P.; Schinke, R. Formation of ozone: Metastable states and anomalous isotope effect. *J. Chem. Phys.* 2003, *119*, 2577– 2589, DOI: 10.1063/1.1587113

16 Babikov, D.; Kendrick, B. K.; Walker, R. B.; T Pack, R.; Fleurat-Lesard, P.; Schinke, R. Metastable states of ozone calculated on an accurate potential energy surface. *J. Chem. Phys.* 2003, *118*, 6298– 6308, DOI: 10.1063/1.1557936

17 Babikov, D.; Kendrick, B. K.; Walker, R. B.; Schinke, R.; Pack, R. T. Quantum origin of an anomalous isotope effect in ozone formation. *Chem. Phys. Lett.*2003, *372*, 686– 691, DOI: 10.1016/S0009-2614(03)00479-2

18 Grebenshchikov, S. Y.; Schinke, R. Towards quantum mechanical description of the unconventional mass-dependent isotope effect in ozone: Resonance recombination in the strong collision approximation. *J. Chem. Phys.* 2009, *131*,181103– 181107, DOI: 10.1063/1.3253994

19 Vetoshkin, E.; Babikov, D. Semiclassical wave packet treatment of scattering resonances: application to the delta zero-point energy effect in recombination reactions. *Phys. Rev. Lett.* 2007, *99*,138301– 138304, DOI: 10.1103/PhysRevLett.99.138301

20 Charlo, D.; Clary, D. C. Quantum-mechanical calculations on pressure and temperature dependence of three-body recombination reactions: Application to ozone formation rates. *J. Chem. Phys.*2004, *120*, 2700– 2707, DOI: 10.1063/1.1635361

21 Charlo, D.; Clary, D. C. Quantum-mechanical calculations on thermolecular association reactions XY+Z+M->XYZ+M: Application to ozone formation. *J. Chem. Phys.* 2002, *117*, 1660– 1672, DOI: 10.1063/1.1485069

22 Ivanov, M. V.; Babikov, D. Mixed quantum-classical theory for the collisional energy transfer and the ro-vibrational energy flow: Application to ozone stabilization. *J. Chem. Phys.* 2011, *134*, 174308, DOI: 10.1063/1.3585690

23 Ivanov, M. V.; Babikov, D. Efficient quantum-classical method for computing thermal rate constant of recombination: Application to ozone formation. *J. Chem. Phys.* 2012, *136*, 184304, DOI: 10.1063/1.4711760

24 Ivanov, M. V.; Babikov, D. On molecular origin of mass-independent fractionation of oxygen isotopes in the ozone forming recombination reaction. *Proc. Natl. Acad. Sci. U. S. A.* 2013, *110*, 17708– 17713, DOI: 10.1073/pnas.1215464110

25 Ivanov, M. V.; Babikov, D. On stabilization of scattering resonances in recombination reaction that forms ozone. *J. Chem. Phys.* 2016, *144*, 154301, DOI: 10.1063/1.4945779

26 Ivanov, M. V.; Schinke, R. Vibrational energy transfer in Ar-O_3 collisions: Comparison of rotational sudden, breathing sphere, and classical calculations.*Mol. Phys.* 2010, *108*, 259– 268, DOI: 10.1080/00268970903397256

27 Xie, T.; Bowman, J. M. Quantum inelastic scattering study of isotope effects in ozone stabilization dynamics. *Chem. Phys. Lett.* 2005, *412*,131– 134, DOI: 10.1016/j.cplett.2005.06.111

28 Ivanov, M. V.; Grebenshchikov, S. Y.; Schinke Intra- and intermolecular energy transfer in highly excited ozone complexes. *J. Chem. Phys.* 2004, *120*, 10015–10024, DOI: 10.1063/1.1712866

29 Ivanov, M. V.; Schinke, R. Temperature dependent energy transfer in Ar-O_3 collisions. *J. Chem. Phys.*2005, *122*, 234318, DOI: 10.1063/1.1927526

30 Hathorn, B. C.; Marcus, R. A. An intramolecular theory of the mass-independent isotope effect for ozone. *J. Chem. Phys.* 1999, *111*, 4087– 4100, DOI: 10.1063/1.480267

31 Hathorn, B. C.; Marcus, R. A. An intramolecular theory of the mass-independent isotope effect for ozone. II. Numerical applications at low pressures using a loose transition state. *J. Chem. Phys.* 2000,*113*, 9497– 9509, DOI: 10.1063/1.1321045

32 Gao, Y. Q.; Marcus, R. A. Strange and unconventional isotope effects in ozone formation.*Science* 2001, *293*, 259– 263, DOI: 10.1126/science.1058528

33 Gao, Y. Q.; Marcus, R. A. On the theory of the strange and unconventional isotopic effects in ozone formation. *J. Chem. Phys.* 2002, *116*, 137– 154, DOI: 10.1063/1.1415448

34 Gao, Y. Q.; Chen, W. C.; Marcus, R. A. A theoretical study of ozone isotopic effects using a modified ab initio potential energy surface. *J. Chem. Phys.* 2002,*117*, 1536– 1543, DOI: 10.1063/1.1488577

35 Dawes, R.; Lolur, P.; Li, A.; Jiang, B.; Guo, H.Communication: Highly accurate ozone formation potential and implications for kinetics. *J. Chem. Phys.*2013, *139*, 201103, DOI: 10.1063/1.4837175

36 Ndengué, S.; Dawes, R.; Wang, X.-G.; Carrington, T.; Sun, Z.; Guo, H. Calculated vibrational states of ozone up to dissociation. *J. Chem. Phys.* 2016, *144*,074302, DOI: 10.1063/1.4941559

37 Teplukhin, A.; Babikov, D. Efficient method for calculations of ro-vibrational states in triatomic molecules near dissociation threshold: application to ozone. *J. Chem. Phys.* 2016, *145*, 114106, DOI: 10.1063/1.4962914

38 Lapierre, D.; Alijah, A.; Kochanov, R.; Kokoouline, V.; Tyuterev, V. Lifetimes and wave functions of ozone metastable vibrational states near the dissociation limit in a full-symmetry approach. *Phys. Rev. A: At., Mol., Opt. Phys.* 2016, *94*, 042514, DOI: 10.1103/PhysRevA.94.042514

39 Xie, W.; Liu, L.; Sun, Z.; Guo, H.; Dawes, R. State-to-state reaction dynamics of $^{18}O+^{32}O_2$ studied by a time-dependent quantum wavepacket method. *J. Chem. Phys.* 2015, *142*, 064308, DOI: 10.1063/1.4907229

40 Sun, Z.; Yu, D.; Xie, W.; Hou, J.; Dawes, R.; Guo, H.Kinetic isotope effect of the $^{16}O + {}^{36}O_2$ and $^{18}O+^{32}O_2$isotope exchange reactions: Dominant role of reactive resonances revealed by an accurate time-dependent quantum wavepacket study. *J. Chem. Phys.* 2015,*142*, 174312, DOI: 10.1063/1.4919861

41 Rao, T. R.; Guillon, G.; Mahapatra, S.; Honvault, P.Differential cross sections and product rovibrational distributions for $^{16}O + {}^{32}O_2$ and $^{18}O + {}^{36}O_2$ collisions.*J. Phys. Chem. A* 2015, *119*, 11432, DOI: 10.1021/acs.jpca.5b08638

42 Teplukhin, A.; Babikov, D. Full-dimensional model of ozone forming reaction: absolute value of recombination rate coefficient, its pressure and temperature dependencies. *Phys. Chem. Chem. Phys.*2016, *18*, 19194– 19206, DOI: 10.1039/C6CP02224C

43 Teplukhin, A.; Babikov, D. Visualization of potential energy function using isoenergy approach and 3D prototyping. *J. Chem. Educ.* 2015, *92*, 305–309, DOI: 10.1021/ed500683g

44 Teplukhin, A.; Babikov, D. Interactive tool for visualization of adiabatic adjustment in APH coordinates for computational studies of vibrational motion and chemical reactions. *Chem. Phys. Lett.*2014, *614*, 99– 103, DOI: 10.1016/j.cplett.2014.09.015

45 Pack, R. T.; Parker, G. A. Quantum reactive scattering in three dimensions using hyperspherical (APH) coordinates. Theory. *J. Chem. Phys.* 1987, *87*,3888, DOI: 10.1063/1.452944

46 Ayouz, M.; Babikov, D. Global permutationally invariant potential energy surface for the ozone-forming reaction. *J. Chem. Phys.* 2013, *138*, 164311, DOI: 10.1063/1.4799915

47 Babikov, D.; Semenov, A.; Teplukhin, A. One possible source of mass-independent fractionation of sulfur isotopes in the Archean atmosphere of Earth.*Geochim. Cosmochim. Acta* 2017, *204*, 388– 406, DOI: 10.1016/j.gca.2017.01.029

48 Teplukhin, A.; Gayday, I.; Babikov, D. Several levels of theory for description of isotope effects in ozone: Effect of resonance lifetimes and channel coupling. *J. Chem. Phys.* 2018, *149*, 164302, DOI: 10.1063/1.5042590

49 Teplukhin, A. *Theoretical study of ozone forming recombination reaction and anomalous isotope effect associated with it*. Ph.D. Dissertation, Marquette University: Milwaukee, WI, 2017.

50 Bunker, P. R. *Molecular symmetry and spectroscopy*; Academic Press: 1979.